Supporting Information for:

Single-step Replacement of an Unreactive C-H Bond by a C-S Bond Using Polysulfide as the Direct Sulfur Source in Anaerobic Ergothioneine Biosynthesis

Ronghai Cheng,[†1] Lian Wu,[†2, 8, 9] Rui Lai,[†1] Chao Peng,[†3] Nathchar Naowarojna,[†1] Weiyao Hu,[1,4] Xinhao Li,[4] Stephen A. Whelan,[1] Norman Lee,[1] Juan Lopez,[1] Changming Zhao,[1,5] Youhua Yong,[2] Jiahui Xue,[6] Xuefeng Jiang,[6] Mark W. Grinstaff,[1,7] Zixin Deng,[5] Jiesheng Chen,[4] Qiang Cui,[1*] Jiahai Zhou,[2*] and Pinghua Liu[1*]

[1]Department of Chemistry, Boston University, Boston, MA 02215, USA.

[2]State Key Laboratory of Bio-organic and Natural Products Chemistry, Center for Excellence in Molecular Synthesis, Shanghai Institute of Organic Chemistry, University of Chinese Academy of Sciences, Shanghai 200032, China.

[3]National Facility for Protein Science in Shanghai, Zhangjiang Lab, Shanghai Advanced Research Institute, Chinese Academy of Science, Shanghai 201210, China.

[4]School of Chemistry and Chemical Engineering, Shanghai JiaoTong University, Shanghai, 200240, China.

[5]Key Laboratory of Combinatory Biosynthesis and Drug Discovery (Wuhan University), Ministry of Education, School of Pharmaceutical Sciences, Wuhan University, Hubei 430072, People's Republic of China.

[6]Shanghai Key Laboratory of Green Chemistry and Chemical Process, East China Normal University, 3663 North Zhongshan Road, Shanghai 200062, P. R. China.

[7]Department of Biomedical Engineering, Boston University, Boston, MA 02215, USA.

[8]Key Laboratory of Synthetic Biology, CAS Center for Excellence in Molecular Plant Sciences, Institute of Plant Physiology and Ecology, Shanghai Institutes for Biological Sciences, Shanghai 200032, China; [9]College of Life Science, University of Chinese Academy of Sciences, Beijing 100049, China.

Corresponding Author

Pinghua Liu: Pinghua@bu.edu, Jiahai Zhou: jiahai@mail.sioc.ac.cn, and Qiang Cui: qiangcui@bu.edu

[†] These authors contributed equally to this work

Index

Supporting Methods **S3**

Supporting Tables **S8**

Supporting Figures **S10**

Supporting Discussion **S33**

References **S36**

Supporting Methods

Protein purification

EanB cells (50 g) were resuspended in 200 mL lysis buffer (100 mM Tris-HCl, 200 mM NaCl, pH 8.0) with 1 mg•mL^{-1} final concentration of lysozyme. The mixture was incubated on ice with shaking for 30 min. Cells were lysed by sonication (505 Sonic Dismembrator) for 50 cycles and at the 20th cycle, DTT was added to cell lysate to 1 mM final concentration. Cell debris was removed via centrifugation at 20,000 rpm for 30 min. at 4 ℃. The supernatant was incubated with 15 mL of Ni Sepharose resin (GE Healthcare). The column was washed with 75 mL of 30 mM imidazole and 1 mM DTT containing lysis buffer, followed by 75 mL of 30 mM imidazole lysis buffer. The protein was eluted by 250 mM imidazole containing lysis buffer and concentrated using ultrafiltration (Millipore). The imidazole was removed from concentrated protein using a G25 Sephadex size-exclusion column (30 × 600 mm). The EanB containing fractions were pooled and concentrated through ultrafiltration. The protein was concentrated to 50 mg•mL^{-1} and stored at -80 ℃.

The mutant constructs were generated using Q5 Site-directed Mutagenesis Kit following suggested protocol (New England Biolabs). The overexpression and purification of the variants were carried out following the protocol of the wild type EanB. Notably, due to the instability of EanB$_{C412\text{-only}}$ mutant, the lysis buffer for the purification of this mutant was changed to 100 mM Tris-HCl, 500 mM NaCl, and 10% glycerol, pH 8.0.

Similar to EanB, the IscS purification was performed under anaerobic condition at 4 ℃ unless otherwise stated. Cells (20 g) were resuspended in 100 mL lysis buffer (100 mM Tris-HCl, 300 mM NaCl, pH 8.0) with lysozyme at 1 mg•mL^{-1} final concentration. The mixture was incubated on ice with shaking for 30 min. Cells were lysed by sonication and PLP was added to 0.1 mM final concentration. Cell debris was removed by centrifugation at 20,000 rpm at 4 ℃ for 30 min. The supernatant was incubated with 15 mL of Ni Sepharose resin. The column was washed with 75 mL lysis buffer supplemented with 30 mM imidazole with 0.1 mM PLP, followed by 75 mL lysis buffer supplemented with 30 mM imidazole. The protein was eluted using lysis buffer supplemented with 250 mM imidazole. Imidazole in the eluted protein was removed following the procedure used in EanB purification. The IscS protein was concentrated to 70 mg•mL^{-1} and stored at -80 ℃. The purified proteins were characterized by SDS-PAGE analysis (**Figure S20**).

Ergothionase was overexpressed and purified similarly. Six grams of cell was suspended in 30 mL of 100 mM Tris-HCl, 300 mM NaCl, pH 8.0 buffer. Lysozyme (30 mg) was added and the mixture was incubated on ice with shaking for 30 min. Cells were lysed by sonication and supernatant was separated from cell debris by centrifugation at 20000 rpm at 4 ℃ for 30 min. Supernatant was loaded onto 5 mL Ni Sepharose resin and incubated with shaking for 30 minutes. Resin was washed with 50 mL of buffer containing 30 mM imidazole and the desired ergothionase was eluted using buffer containing 200 mM imidazole. The protein was concentrated by ultrafiltration and dialyzed against 2 L of 100 mM Tris-HCl, 50 mM NaCl, pH 8.0 buffer for 2 hr, and then dialyzed again in 2 L fresh buffer overnight at 4 ℃. Protein after dialysis was concentrated to 20 mg•mL^{-1} and stored at -80 ℃. The purified protein was characterized by SDS-PAGE analysis (**Figure S21**).

Characterize the dominant polysulfide species in the EanB reaction mixture

The dominant polysulfide species in the EanB-K_2S_x reaction mixture was determined by following a reported procedure.[1] A 6-mL reaction containing 0.15 mM EanB, 1.5 mM K_2S_x, and 1.5 mM hercynine in 50 mM KPi pH 8.0, was set up anaerobically at room temperature. A 1-mL aliquot of the reaction mixture was withdrawn at 0, 5, 10, and 30 min., and mixed with 4 mL of MeOH. Then, 60 μL of methyl triflate was added

to the sample-MeOH mixture. Polysulfide was salting out by adding 8 mL of 375 mM sodium sulfate to the mixture. Polysulfide was extracted twice using 100 μL of n-dodecane each time. Then, 40 μL of the extracted solution was used for HPLC analysis (90% MeOH, 10% H_2O, 0.5 mL min^{-1}) on C18 column (4.6 x 250 mm, 5 μm, YMC-triart).

To identify the chain length of polysulfide, Me_2S_3 standard was diluted 2000-fold and analyzed under the same HPLC conditions. The species present in commercially available K_2S_x stock solution was also determined.[2] 10 μL of 10 mg of K_2S_x was dissolved in 1 mL of 50 mM pH 8.0 KPi buffer. The mixture was then mixed with 90 μL MeOH and treated with 10 μL methyl triflate. The derivatized polysulfide was subjected to HPLC analysis using the same conditions.

Protein expression and purification for crystallization

The full-length wild-type EanB from *C. limicola* was cloned in vector pSJ5, with 8xHis and TrxA fusion tag. The protein was expressed in *E. coli* BL21(DE3) in YT medium in the presence of 100 μg•mL^{-1} ampicillin. Expression was induced by 0.4 mM IPTG when OD_{600} nm reached 1.0-1.5. After growing for 16-18 hr at 16 ℃, the cells were harvested by centrifugation. The $EanB_{Y353A}$ was cloned in the same vector pSJ5 and overexpressed by the same method.

The cells were suspended in buffer 25 mM Tris-HCl pH 8.0, 500 mM NaCl and lysed by high-pressure cell homogenizer (400-600 bar). Cells debris was removed by centrifugation at 18,000 rpm for 30 min. at 4 ℃. Supernatant was loaded to a Ni-NTA affinity column and non-specific binding proteins were removed by stepwise elution with lysis buffer containing different concentration of imidazole (15 mM, 30 mM, 45 mM). The EanB containing His-tag was eluted using lysis buffer with 300 mM imidazole. The pure protein was collected for fusion tag cleavage at 16 ℃ with TEV 10000 U, for 2 hr. The mixture was then reloaded to a Ni-NTA affinity column again to remove the TEV enzyme and fusion tag. The flow-through containing EanB protein without tag was collected, concentrated to 2 ml using Amicon ultra filter units (Millipore) with a 30 kDa molecular weight cutoff. The concentrated protein was then loaded to a high-load 16/600 superdex 200 column (GE Healthcare) in a buffer containing 25 mM Tris-HCl, pH 8.0, 150 mM NaCl. The peak fraction was collected and analyzed by SDS-PAGE. The pure protein was collected and concentrated for crystallization. Only the protein for EanB•hercynine complex crystallization was purified by this method in aerobic condition.

The mutants $EanB_{Y353A}$ were purified under anaerobic condition. After harvesting, the cells were flash-cooled in liquid nitrogen, transferred into anaerobic box, and resuspended in lysis buffer (25 mM Tris-HCl pH 8.0, 500 mM NaCl). The cells were lysed by ultrasonic cells crusher with addition of 30 mg lysozyme per 10 g cells. Cell debris was removed by centrifugation at 7800 rpm for 1 hr. Supernatant was loaded to a Ni-NTA column and eluted by stepwise using lysis buffer with different concentration of imidazole (15 mM,30 mM,45 mM). The EanB protein was eluted with lysis buffer containing 300 mM imidazole. The pure protein was concentrated by centrifugal filter (Amicon Ultra-15) and buffer exchanged to 25 mM Tris-HCl pH 8.0, 150 mM NaCl for fusion-tag cleavage by incubating with 10000 U TEV enzyme for 1.5-2 hr at 16 ℃. Then, NaCl was added to the mixture to 500 mM final concentration before loading to a Ni-NTA affinity column to remove the TEV enzyme and fusion tag. The flow-through which was the protein without 8xHis and TrxA fusion tag was collected, concentrated and exchanged into a buffer containing 25mM Tris-HCl, pH 8.0, 150 mM NaCl for crystallization.

Single-turnover reaction of EanB variants

The activity of $EanB_{C412S}$, $EanB_{Y353A}$, and $EanB_{Y353F}$, were monitored using ^1H NMR assay for single-turnover reaction. Under anaerobic condition, a 1.5-mL reaction containing 0.5 mM EanB variants, 2.5 mM hercynine, and 7.5 mM K_2S_x in 100 mM Tris-HCl, 50 mM NaCl, pH 8.0., was set up at room temperature for 8 hours. Protein was precipitated by addition of 250 μL of 6 M HCl and precipitated protein was removed via centrifugation. The samples were analyzed by mass spectrometry to quantify the production of ergothioneine. The remaining of reaction mixture was neutralized and lyophilized. The product formation was analyzed by ^1H-NMR. Additionally, the reaction was repeated twice.

Quantification of ergothioneine from EanB single-turnover reactions

The amount of ergothioneine production from EanB-IscS, EanB-polysulfide, $EanB_{C412\text{-}only}$-IscS, and $EanB_{C412\text{-}only}$-polysulfide single-turnover reaction was quantified using ultra-high-performance liquid chromatography combined with mass spectrometry (UPLC-MS). Hercynine-d_3 (HER-d_3) and ergothioneine-d_3 (ERG-d_3) were used as internal standards for hercynine and ergothioneine, respectively. Standards were dissolved in 50% CH_3OH/H_2O at a concentration of 10 mM as stock solutions and stored at 20 °C. The working solutions of hercynine and ergothioneine for calibration curve were diluted with their stock solutions with 50% CH_3OH/H_2O at 9 different concentration levels in the range of 20–8000 nM for hercynine and 100-40000 nM for ergothioneine. The working solutions of internal standards (HER-d3 or ERG-d3) were prepared at a concentration of 20000 nM in 50% CH_3OH/H_2O. Finally, the calibration curve samples were prepared by mixing the working solutions of the compounds and internal standard at a ratio of 1:1.

The UPLC-MS analysis was performed on an Agilent 1290 UPLC (Agilent, USA) coupled to an AB Sciex 6500 QTRAP mass spectrometer (AB Sciex, USA) with the electrospray ionization (ESI) source. A Waters ACQUITY UPLC BEH HILIC column (1.7 μm, 2.1 × 100 mm) was used for separation with flow rate at 0.4 mL•min^{-1} and column temperature at 45 °C. The mobile phases were comprised of (A) 0.2% formic acid and 10 mM ammonium acetate in 50% acetonitrile and (B) 0.2% formic acid and 10 mM ammonium acetate in 95% acetonitrile. The gradient elution was 90% B kept for 1.0 min., followed by a linear gradient to 5% B during 7.0 min. and maintained 5% B to 10.0 min., then increased to 90% B in 10.1 min. and maintained for 2.9 min. Multiple Reaction Monitoring (MRM) was used to monitor the compounds and internal standard in the positive ion mode. Data acquisition and processing were performed using Analyst (version 1.6, Applied Biosystems SCIEX). The quantification was performed for at least three independent trials.

Quantification of persulfide content of EanB by cyanolysis

The persulfide content of $EanB_{C412\text{-}only}$ for single-turnover reaction was determined following reported procedure.[3,4] Under anaerobic condition, a 150-μL portion of 396 μM of $EanB_{C412\text{-}only}$ in 100 mM Tris-HCl, 50 mM NaCl, pH 8.0 was treated with 7.5 μL of 1 M KCN and incubated at room temperature for 2 hours. Then, 75 μL of 15% formaldehyde was added to the mixture to remove excess cyanide. Subsequently, a 225-μL portion of ferric nitrate solution (1 g $Fe(NO_3)_3x\ 9H_2O$, 13 mL H_2O, 2 mL HNO_3 (65%)) was added to from ferric thiocyanate. Absorbance at 460 nm was measured. The standard curve using potassium thiocyanate was constructed (50 – 200 μM). Each reaction was performed in duplicate. Using molar extinction coefficient (ε_{460}) of 2773 ± 0.1071 $\mu M^{-1}cm^{-1}$ for potassium thiocyanate, the persulfide content of as-purified $EanB_{C412\text{-}only}$ was 28%.

Tandem mass spectrometry analysis

Prior to tandem mass spectrometry, the protein samples from single-turnover reaction were alkylated. Then, the mixture was digested by Sequencing Grade Modified Trypsin (Promega) at 37 ℃ for overnight. The tryptic digested peptides were desalted and loaded on an in-house packed capillary reverse-phase C18 column (25 cm length, 100 μM ID x 360 μM OD, 1.9 μM particle size, 120Å pore diameter) connected to an Easy LC 1200 system. The samples were analyzed with a 120min-HPLC gradient from 5% to 35% of buffer B (buffer A: 0.1% formic acid in water; buffer B: 0.1% formic acid in 80% acetonitrile) at 300 nL•min^{-1}. The eluted peptides were ionized and directly introduced into a Q-Exactive mass spectrometer using a nano-spray source. Survey full-scan MS spectra (from m/z 300–1800) were acquired in the Orbitrap analyzer with resolution r = 70,000 at m/z 400. Protein identification and protein post-modification identification were done with Proteome Discoverer2.2.

Mass spectrometry analysis of cysteine polysulfide

Cysteine polysulfide was prepared anaerobically by mixing 100 mM cysteine with 100 mM S_8 in a 1-mL water at room temperature for 1 hour. Then, 10 mM cysteine polysulfide was alkylated with 100 mM iodoacetamide in a 5-mL reaction shielded from light at room temperature for 1 hour. The mixture was subjected to LC/MS analysis (linear gradient from 5% to 90% MeOH with 0.1% formic acid for 30 minutes, 0.5 mL min^{-1}, 10 μL sample was injected) using C18 column (YMC-triart, 5 μm, 4.6 × 100 mm). In characterization of cysteine polysulfide by mass spectrometry, four different alkylated polysulfide species were observed: alkylated cysteine, alkylated cysteine disulfide, alkylated cysteine trisulfide, and alkylated cysteine tetrasulfide.

Calculated value for alkylated cysteine $[M+H]^+$ form (positive mode) was *m/z* 179.0485 and found *m/z* 179.0486.

Calculated value for alkylated cysteine disulfide $[M+H]^+$ form (positive mode) was *m/z* 211.0206 and found *m/z* 211.0206.

Calculated value for alkylated cysteine trisulfide $[M+H]^+$ form (positive mode) was *m/z* 242.9926 and found *m/z* 242.9928.

Calculated value for alkylated cysteine tetrasulfide $[M+H]^+$ form (positive mode) was *m/z* 274.9650 and found *m/z* 274.9647.

Mass spectrometry analysis of GSH polysulfide

GSH polysulfide was prepared by treating 100 mM of GSH with 100 mM S_8 in 1 mL of H_2O. The reaction was incubated at room temperature for 60 minutes. Then, glutathione polysulfide solution was derivatized by iodoacetamide. A 1-mL reaction containing 10 mM glutathione polysulfide and 100 mM iodoacetamide in 10 mM pH 8.0Tris-HCl buffer, was set up under dark at room temperature for 1 hour. The sample was subjected to LC/MS analysis using Jupiter Proteo 90A column from phenomenex (linear gradient from 5% to 95% MeOH with 0.1% formic acid for 30 minutes at a rate of 0.1 mL per min.) 10 μL of polysulfide sample was used in the analysis. Three alkylated products were detected in mass spectrometry: GSH, GSH disulfide, and GSH trisulfide. This experiment was repeated twice. The fragments of glutathione polysulfide species were detected by Thermofisher™ LTQ XL™ Linear Ion Trap Mass Spectrometer.

Calculated *m/z* ratio for alkylated GSH $[M+H]^+$ form (positive mode) was 365.1125 and found at 365.1124.

Calculated *m*/*z* ratio for alkylated GSH disulfide $[M+H]^+$ form (positive mode) was 397.0846 and found at 397.0845.

Calculated *m*/*z* ratio for alkylated GSH trisulfide $[M+H]^+$ form (positive mode) was 429.0567 and found at 429.0566.

Supporting Tables

Table S1. X-ray data collection and refinement statistics of EanB and complex structures.

Name	EanB	EanB•hercynine	EanB with hercynine C412 persulfide	Y353A with tetrahedral intermediate	Y353A with ergothioneine
PDB ID	6KTX	6KTW	6KTV	6KU2	6KU1
Data collection					
Beamline	SSRF-BL18U1	SSRF-BL18U1	SSRF-BL18U1	SSRF-BL19U1	SSRF-BL19U1
Wavelength (Å)	0.97918	0.97930	0.97930	0.97791	0.97911
Space group	$P2_12_12$	$P2_12_12$	$P2_12_12$	$P2_1$	$P2_1$
Unit cell parameters (Å,◦)	a=88.6 b=111.4 c=60.3 α=β=γ=90	a=88.5 b=112.0 c=60.6 α=β=γ=90	a=88.7 b=112.8 c =119.3 α=β=γ=90	a=62.7 b=88.2 c =90.8 α=γ=90, β=90.3	a=62.7 b=88.0 c =90.6 α=γ=90, β=90.5
Resolution (Å)[a]	50-2.17(2.21-2.17)	50-1.94(1.97-1.94)	50-2.20(2.24-2.20)	50-2.34(2.38-2.34)	45.28(2.32-2.25)
No. of measured reflections	287947	467154	381465	279466	320965
No. of unique reflections	30763 (1457)	45192(2205)	31581 (1530)	41635(2048)	46743(4266)
Redundancy[a]	9.4(7.2)	10.3(10.5)	12.1(8.0)	6.7(6.4)	6.9(6.4)
Completeness (%)[a]	99.6(95.2)	99.8(100.0)	99.8(96.7)	99.5(99.7)	99.9(99.9)
Average (I/σ)[a]	9.5(1.8)	11.3(2.0)	12.9(1.6)	14.7(1.6)	11.2(2.0)
R_{merge} (%)[a,b]	0.213(0.794)	0.447(3.011)	0.199(1.041)	0.139(0.896)	0.141(1.019)
Refinement					
Resolution(Å)[a]	41.7-2.2	41.3-1.9	45.7-2.2	45.4-2.3	36.9-2.3
No. of reflections (work/free)	30108(1460)	44295(2237)	30079(1491)	39334(1890)	46699(2362)
R_{work}/R_{free}[c]	0.1655/0.2131	0.1566/0.1932	0.1665/0.2012	0.1728/0.2291	0.1687/0.2119
No. of non-H atom					
protein	3475	3470	3459	6859	6819
Waters	224	422	226	305	353
ligand	71	42	133	50	76
Avg. B-factor (A^2)	35.5	23.3	34.6	34.7	38.0
Bond lengths (Å)	0.004	0.013	0.007	0.007	0.008
Bond angles (◦)	0.609	1.092	0.818	0.858	0.899
Ramachandran favored (%)	96.5	96.5	97.42	95.38	95.1
Ramachandran allowed (%)	3.5	3.5	2.58	4.5	4.9
Ramachandran outlier (%)	0.00	0.00	0.00	0.12	0

[a] Numbers in parentheses are values for the highest-resolution shell.

[b] $R_{merge} = \Sigma_{hkl}\Sigma_i|I_i - \langle I\rangle|/\Sigma_{hkl}\Sigma_i|\langle I\rangle|$, where I_i is the intensity for the *i*th measurement of an equivalent reflection with indices h, k, and l.

[c] R_{free} was calculated with the 5% of reflections set aside randomly throughout the refinement.

Table S2. Proton affinities (in kcal•mol^{-1}) of small molecules representing the proton donors/acceptors in the reactions of interest (see **Figure S16b**).

	DFTB3	*B3LYP/6-311++G(d,p)*	*B3LYP-D3/6-311++G(d,p)*	*G3B3*
4-methyl-phenol (a and b)	358.3	352.0	352.5	354.4
1,3-H imidazole (c and d)	240.9	233.2	233.7	232.7
1,3-H imidazole (d and e)	248.9	259.6	260.1	259.4
1,3-H imidazole (with modified C-H repulsive potential	257.8	259.6	260.1	259.4
1,3-H 2-S "imidazole" (f and g)	174.2	164.3	165.1	165.2

Table S3. Relative electronic energies (ΔE, kcal•mol^{-1}) and key distances (Å) of models shown in **Figure S16c** optimized at CPCM/B3LYP-D3/6-31G(d,p) level of theory in comparison to geometries from DFTB3/MM metadynamics simulations and single point energy calculations conducted at CPCM/B3LYP-D3/6-311++G(d,p) level of theory.

	ΔE(B3LYP-D3/6-31G(d,p)	**ΔE(B3LYP-D3/6-311++G(d,p)**	***r*(S…S)**	***r*(S…ε-C)**	***r*(N…O$_{Tyr353}$)**	***r*(ε-C…O$_{Tyr353}$)**	***r*(ε-H…ε-C)**	***r*(ε-H… O$_{Tyr353}$)**
RS	0.0	0.0	2.12	3.42	3.63	3.37	1.08	2.70
RS$_{DFTB3/MM}$	N/A	N/A	2.15±0.06	3.44±0.17	3.06±0.17	2.70±0.20	1.08±0.00	2.36±0.30
IM-1	10.4	12.5	2.11	3.30	3.73	2.82	1.11	1.74
IM-1$_{DFTB3/MM}$	N/A	N/A	2.20±0.12	2.97±0.22	3.55±0.17	2.62±0.12	1.26±0.10	1.39±0.21
TS$_{IM-1\ to\ IM-3}$	14.8	18.0	2.11	3.23	3.55	2.58	1.39	1.20
IM-3	13.9	16.7	2.12	3.20	3.67	2.70	1.66	1.05
IM-3$_{DFTB3/MM}$	N/A	N/A	2.16±0.07	3.12±0.23	4.03±0.25	3.09±0.16	2.13±0.16	0.99±0.03
TS$_{IM-3\ to\ PS}$	22.1	24.6	2.38	2.27	4.02	3.07	2.12	0.98
TS$_{IM-1\ to\ PS}$	26.5	30.1	2.22	2.34	3.63	2.58	1.39	1.20
PS	-11.5	-7.3	4.01	1.71	4.25	3.92	3.14	0.99
PS$_{DFTB3/MM}$	N/A	N/A	3.33±0.15	1.75±0.04	4.20±0.33	3.27±0.24	2.39±0.23	0.99±0.03

Supporting Figures

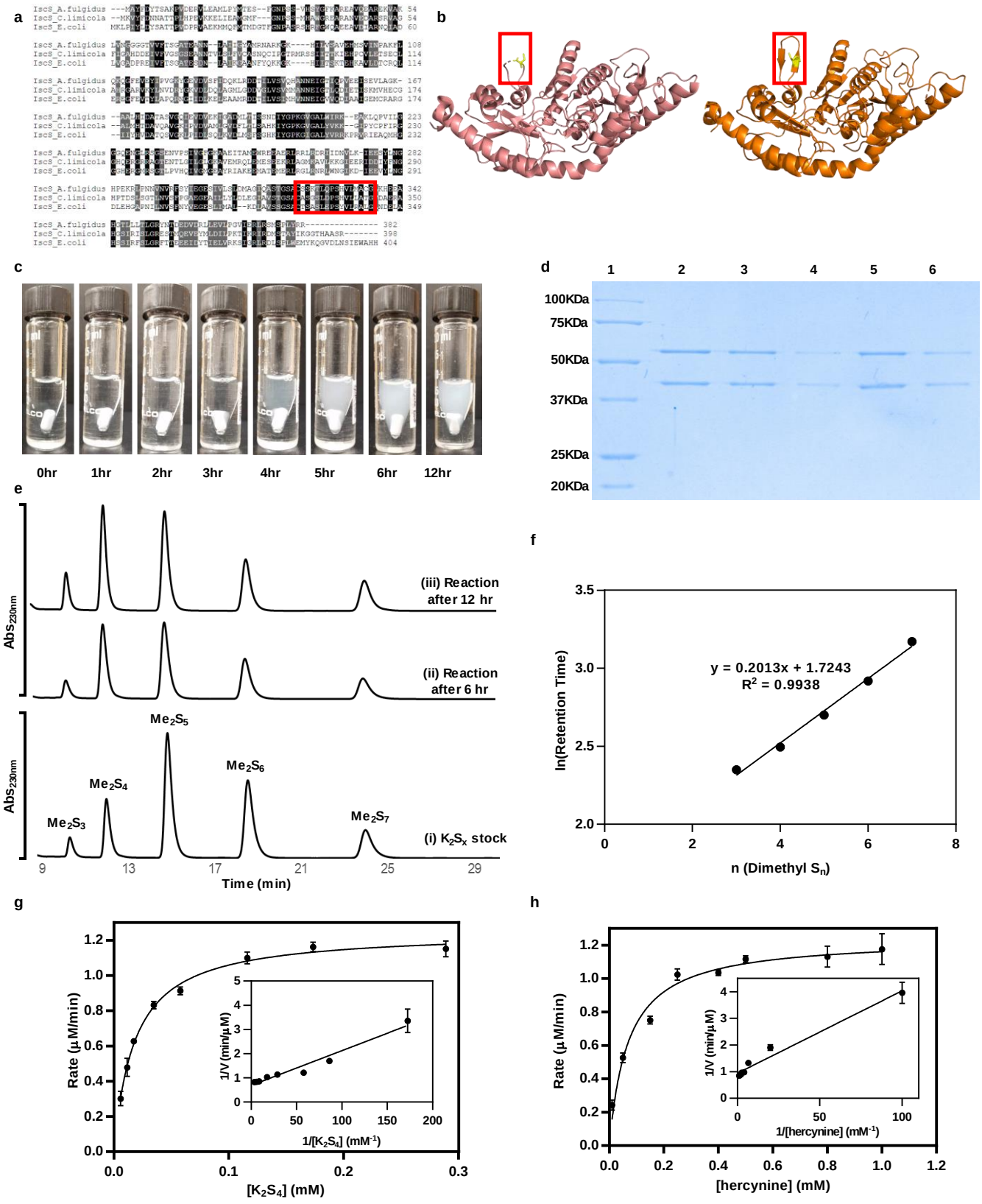

Figure S1 IscS vs polysulfide as the EanB sulfur source. (a) Sequence alignment of IscS from three different species. The active site loop is highlighted in the red box. **(b)** Structural information. *E. coli* IscS

crystal structure (pink color, PDB code: 3lvk) and the structural model of *C. limicola* IscS (accession number: WP_012467067.1, orange color predicted by Phyre2). The loops containing the active site cysteine residue are highlighted in red boxes and the active site cysteines are shown in yellow sticks. **(c)** Pictures of the IscS-EanB reaction overtime. The reaction (1.2-mL) contained 2 μM EanB, 2 μM IscS, 1 mM hercynine, and 1 mM cysteine in 50 mM KPi, pH 8.0, under anaerobic condition. At the end of the reaction, significant amount of precipitate was observed (e.g., 5 – 12 hr). The photos were taken by R. Cheng. **(d)** SDS-PAGE analysis of the precipitate and supernatant of the reaction in **(c)** collected at hour 6 and hour 12. The order of the samples are: marker (1), supernatant at the beginning of the reaction (2), supernatant at hour 6 (3), precipitate at hour 6 (4), supernatant at hour 12 (5), and precipitate at hour 12 (6). By taking the dilution factor into consideration, the amount of proteins in lanes 4 and 6 represent ~1 and 2% of the total protein used in the reaction, respectively (detailed calculation is shown in method section). **(e)** HPLC analysis of the precipitates collected from reaction in **(c)** demonstrated the presence of sulfur-based product. The precipitate was treated with 20 μL of 100 mM Na_2S and after incubation at room temperature for 0.5 hour, the sample was derivatized with methyl triflate and subjected to HPLC analysis. The derivatized polysulfides were monitored by detecting absorbance at 230 nm. Derivatized polysulfide was successfully detected from EanB-IscS reaction mixture. This experiment provides evidence supporting the production of elementary sulfur in the IscS-EanB reaction. **(f)** Standard curve of chain length of polysulfide species was based on a literature procedure.[23] **(g)-(h)** Steady-state kinetic analysis of EanB-catalysis using polysulfide as the sulfur donor: hercynine concentration dependence **(g)** and polysulfide concentration dependence **(h)**. The kinetic parameters are: k_{cat} of 0.68 ± 0.01 min.$^{-1}$, K_m of 69.7 ± 8.7 μM for hercynine, and K_m of 18.1 ± 1.2 μM for polysulfide.

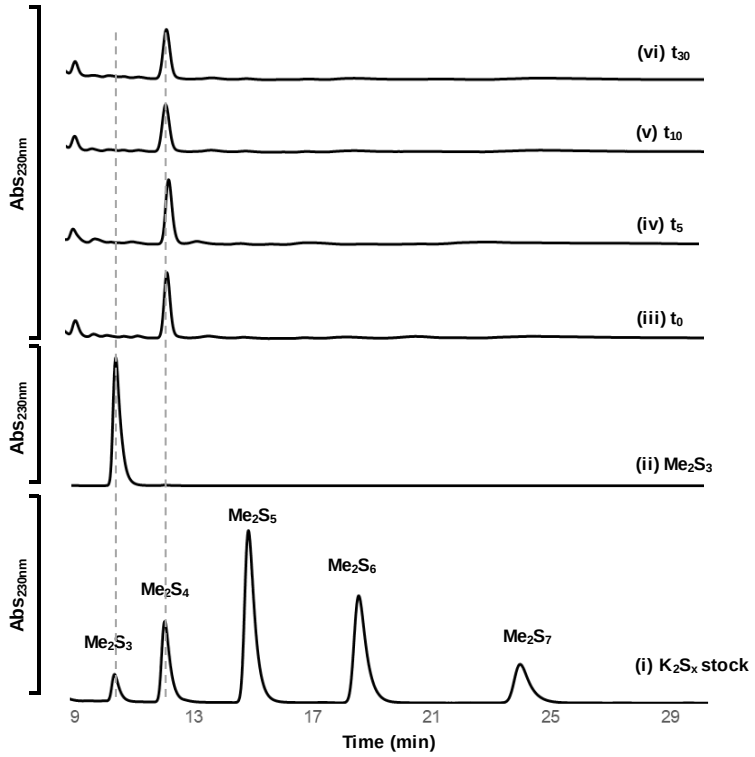

Figure S2 EanB catalysis using polysulfide as the direct sulfur source. HPLC analysis of K_2S_x stock solution after it was derivatized by methyl triflate (trace i) and Me_2S_3 solution (trace ii) serve as standard to assign the identity of polysulfide according to literature procedure.[1,2] The reaction mixture (6-mL reaction) contained 0.15 mM EanB, 1.5 mM K_2S_x, and 1.5 mM hercynine in 50 mM KPi pH 8.0 buffer and the reaction was run under anaerobic condition. Aliquots (1-mL each) of the reaction mixture were withdrawn at 0, 5, 10, and 30 min., respectively. After treatment with methyl triflate and extraction with n-dodecane, the mixture was subjected to HPLC analysis (appearance of derivatized polysulfide was monitored by detecting absorbance at 230 nm), which shows that the dominant species of polysulfide under our assay condition is S_4^{2-}.

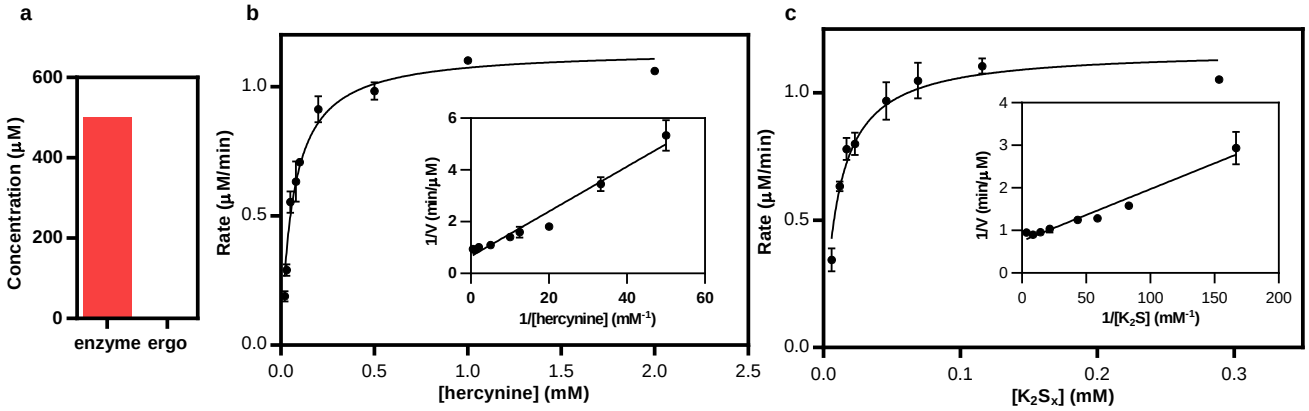

Figure S3 Characterization of EanB Cys412 variants. (a) Mass spectrometry analysis of the amount of ergothioneine produced from $EanB_{C412S}$ variant single-turnover reaction using polysulfide as the direct sulfur source. In this reaction, no ergothioneine is produced. **(b-c)** Steady-state kinetic characterization of $EanB_{C412\text{-only}}$ variant using K_2S_x as the direct sulfur source: hercynine concentration dependence **(a)** and polysulfide concentration dependence **(c)**. The kinetic parameters of $EanB_{C412\text{-only}}$ variant are: k_{cat} of 0.15 ± 0.01 min.$^{-1}$, K_m of 65.9 ± 3.4 μM for hercynine, and K_m of 10.4 ± 1.0 μM for polysulfide.

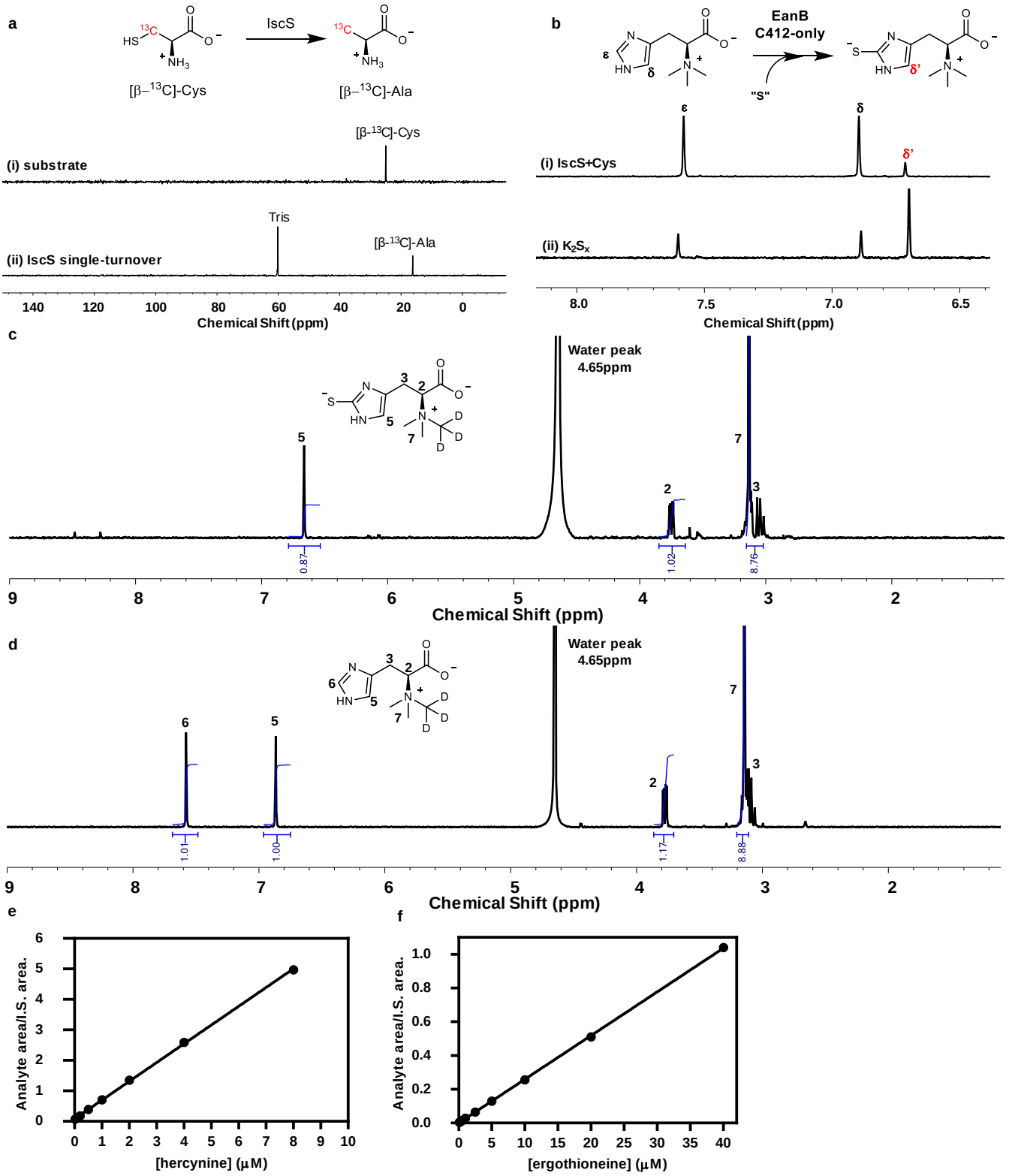

Figure S4 Single-turnover reactions of EanB$_{C412\text{-only}}$ variant and quantification of ergothioneine by mass spectrometry using ergothioneine-*d*$_3$ as an internal standard. (a) ^{13}C NMR spectrum of IscS single-turnover reaction showed that the substrate [β-^{13}C]-Cys (δ 24.97, trace i) is converted to [β-^{13}C]-Ala (δ 16.18, trace ii). **(b)** ^{1}H NMR of EanB$_{C412\text{-only}}$ reaction shows that ergothioneine is produced (δ 6.70) under multiple-turnover assay when IscS with cysteine and polysulfide are the sulfur source (trace i and ii). **(c)** ^{1}H NMR spectrum of ergothioneine-*d*$_3$ used for mass spectrometry quantification. (500 MHz, D_2O): δ 3.00-3.14

(m, 8H), δ 3.74 (dd, J=3.8, 11.8 Hz, 1H), δ 6.63 (s, 1 H). **(d)** ^{1}H NMR of hercynine-d_3 used for mass spectrometry quantification. (500 MHz, D_2O): δ 3.08-3.16 (m, 8H), δ 3.77 (dd, J=4.4, 11.0 Hz, 1H), δ 6.86 (s, 1 H), δ 7.58 (s, 1 H). **(e) – (f)** Standard curve of ergothioneine **(e)** and hercynine **(f)** used in product quantification by mass spectrometry.

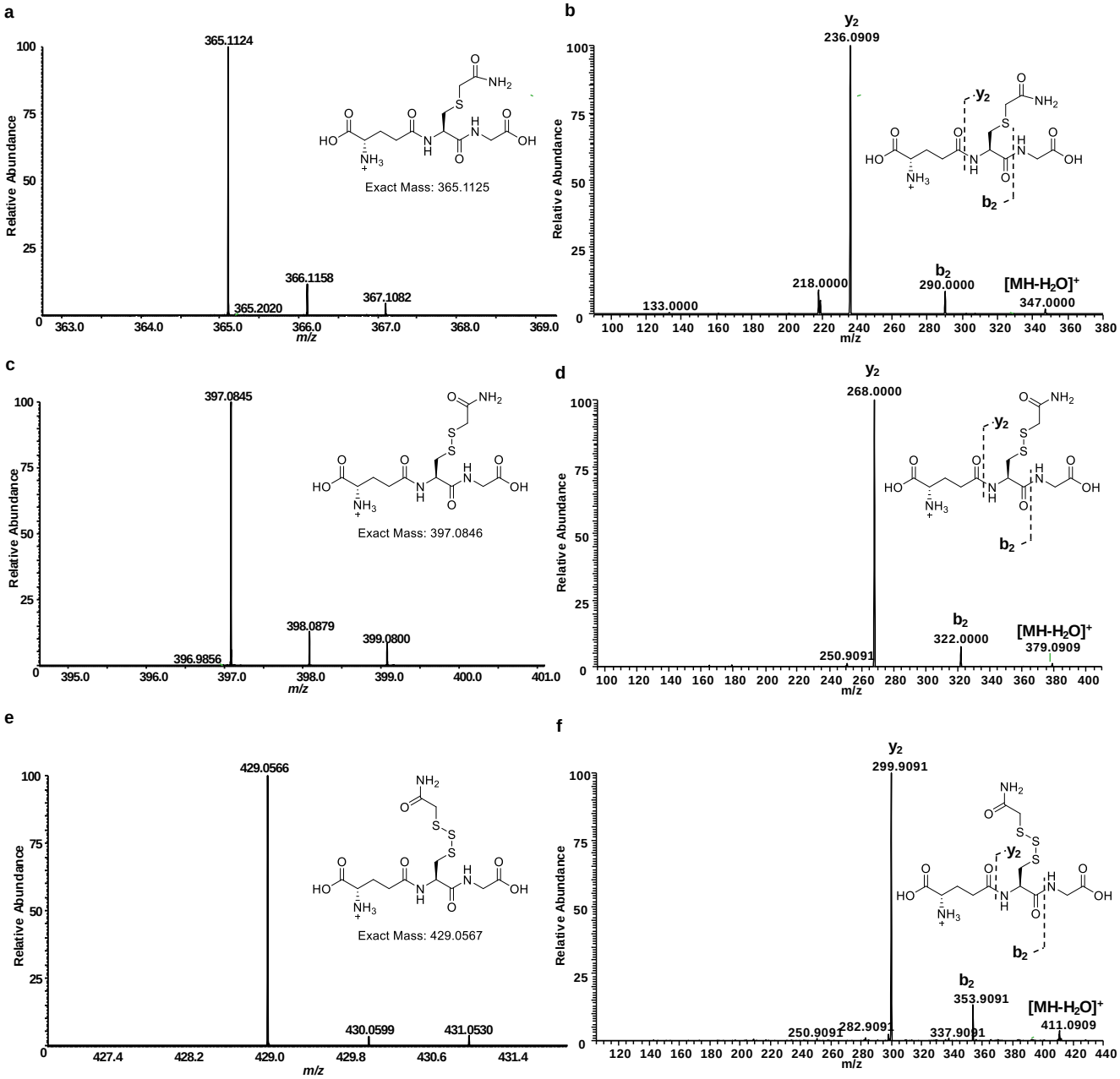

Figure S5 Characterization of GSH polysulfides. GSH polysulfide by obtained by treating 100 mM S_8 with 100 mM GSH in a 1-mL water at room temperature for 1 hour. The sample was then alkylated using iodoacetamide before subjected to LC/MS analysis showing three alkylated products: GSH, GSH disulfide, and GSH trisulfide. **(a)** Calculated *m*/*z* ratio for alkylated GSH $[M+H]^+$ form (positive mode) was 365.1125 and found at 365.1124. **(b)** Tandem mass spectrum of alkylated glutathione **(c)** Calculated *m*/*z* ratio for alkylated GSH disulfide $[M+H]^+$ form (positive mode) was 397.0846 and found at 397.0845. **(d)** Tandem mass spectrum of alkylated glutathione persulfide **(e)** Calculated *m*/*z* ratio for alkylated GSH trisulfide $[M+H]^+$ form (positive mode) was 429.0567 and found at 429.0566. **(f)** Tandem mass spectrum of alkylated glutathione trisulfide.

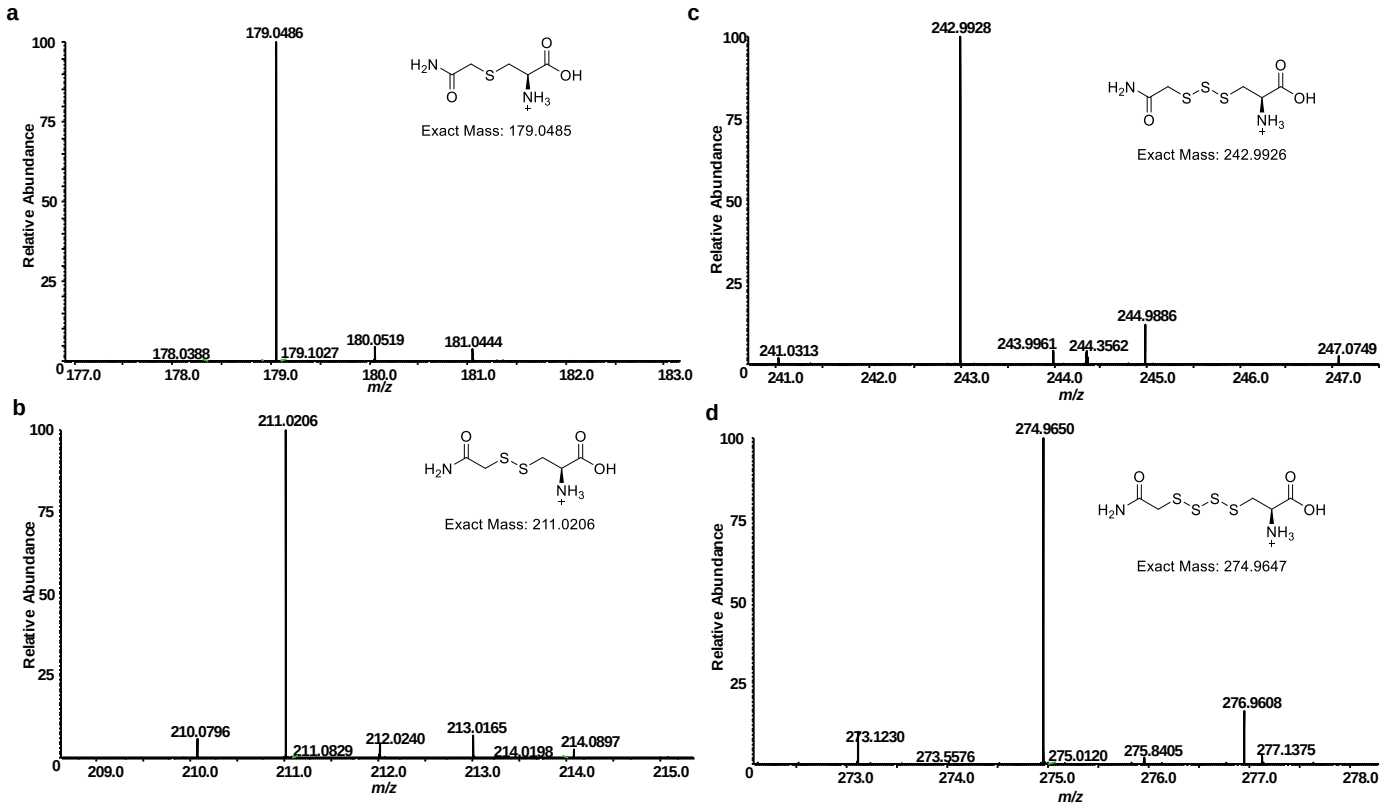

Figure S6 Mass spectrometry analysis of cysteine polysulfides. Cysteine polysulfide by obtained by treating 0.1 mmol S_8 with 0.1 mmol cysteine in a 1-mL water at room temperature for 1 hour. The sample was then alkylated using iodoacetamide before subjected to LC/MS analysis showing four different alkylated polysulfide species: alkylated cysteine, alkylated cysteine disulfide, alkylated cysteine trisulfide, and alkylated cysteine tetrasulfide. **(a)** Calculated value for alkylated cysteine $[M+H]^+$ form (positive mode) was *m/z* 179.0485 and found *m/z* 179.0486. **(b)** Calculated value for alkylated cysteine disulfide $[M+H]^+$ form (positive mode) was *m/z* 211.0206 and found *m/z* 211.0206. **(c)** Calculated value for alkylated cysteine trisulfide $[M+H]^+$ form (positive mode) was *m/z* 242.9926 and found *m/z* 242.9928. (d) Calculated value for alkylated cysteine tetrasulfide $[M+H]^+$ form (positive mode) was *m/z* 274.9650 and found *m/z* 274.9647.

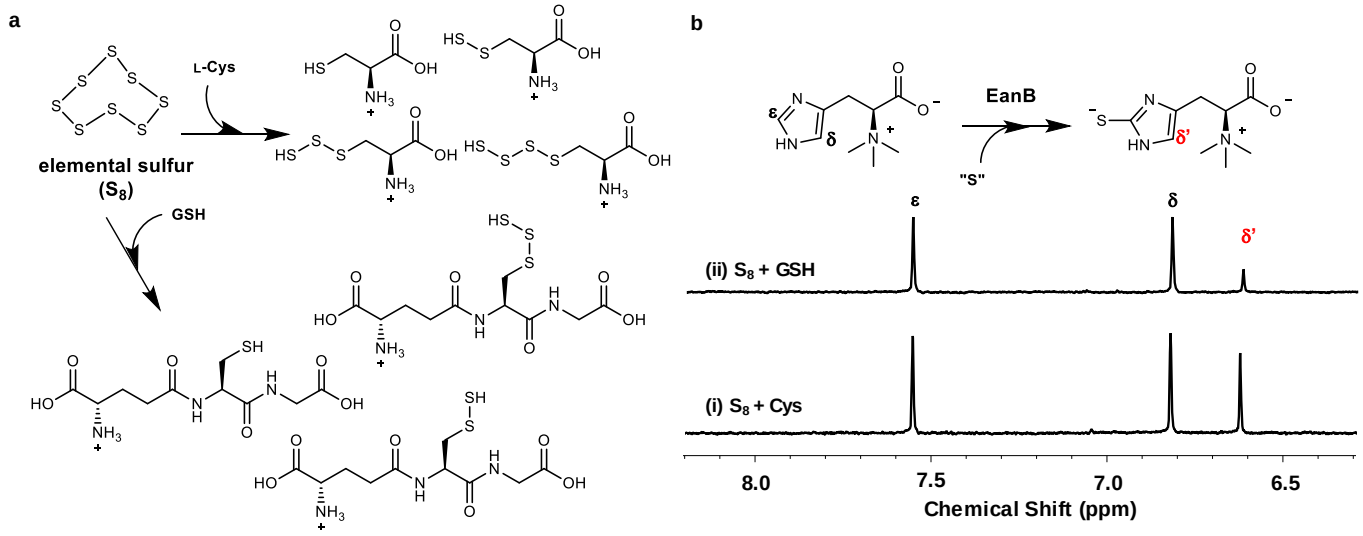

Figure S7 Characterization of EanB reactions using two more polysulfide forms. (a) glutathione (GSH) polysulfide and cysteine polysulfide were obtained by treating elemental sulfur (S_8) with GSH and L-Cys, respectively. The products were characterized by mass spectrometry. **(b)** ^{1}H-NMR analysis of the EanB reaction shows the production of ergothioneine (δ 6.62) when either cysteine polysulfide (trace i), or GSH polysulfide (trace ii) was used as the direct sulfur source.

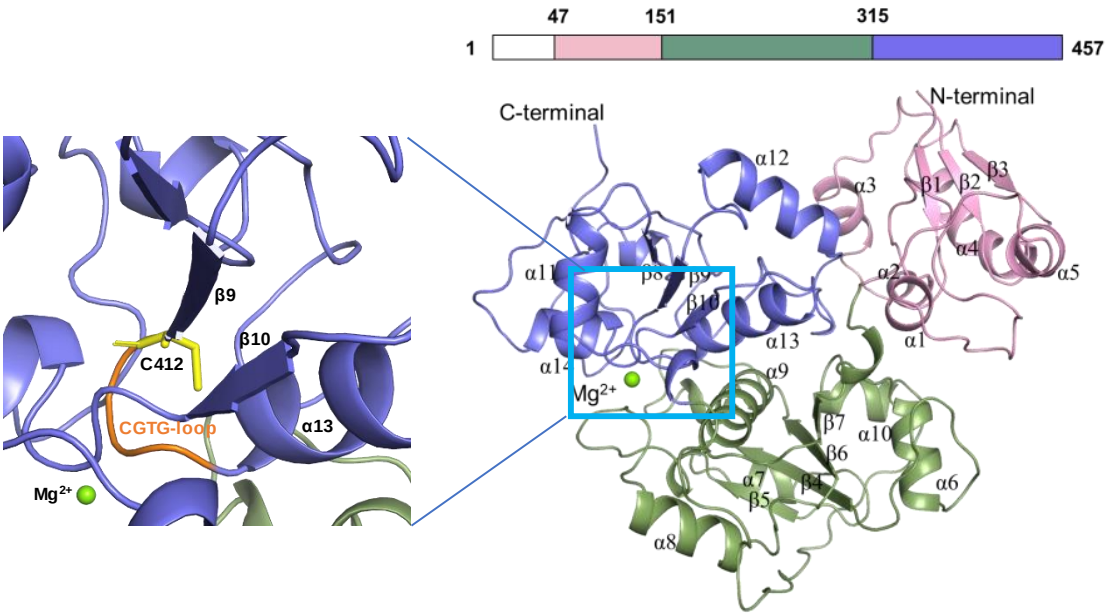

Figure S8 Overall structure of EanB. EanB consists of three rhodanese-like domains. Residues 47-150 are colored pink, residues 151-314 are colored green, and residues 315-457 are colored slate. The active site residues are mainly located at the *C*-terminal domain, while the catalytic residue Cys412 is located on a CGTG-loop like other rhodaneses (zoom-in window).

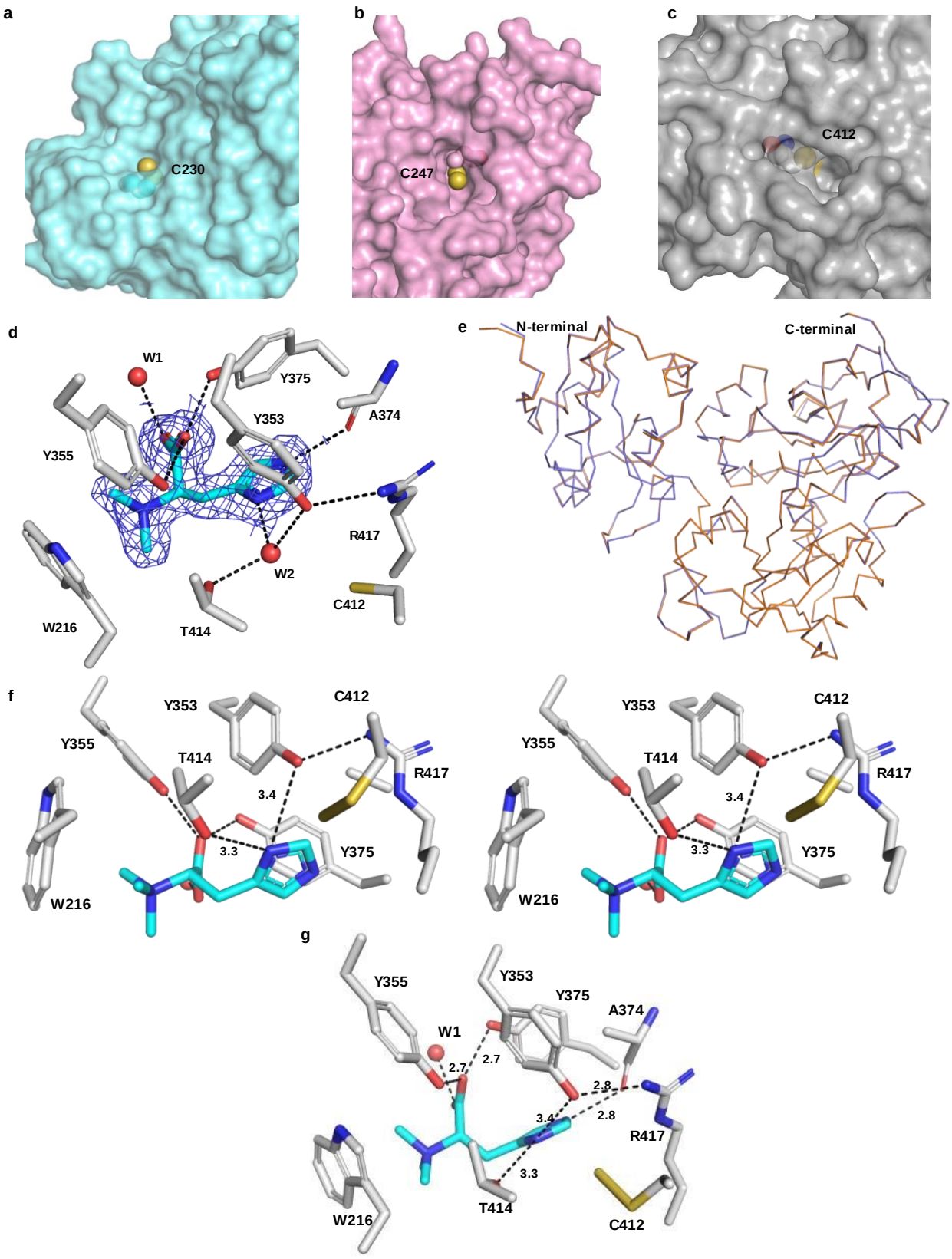

Figure S9 Comparison of EanB and other rhodaneses. (a-c) Surface representation of active site cysteine residues in EanB and two rhodaneses (RhdA and Rhobov). **(a)** The catalytic Cys230 in RhdA (PDB: 1E0C) is close to the surface (shown in yellow sphere). **(b)** The catalytic Cys247 (shown as sphere) in Rhobov (PDB: 1RHD) is solvent-accessible and exposed. **(c)** The active site shows a buried Cys412 residue (shown

in sphere) is located at the bottom of ~ 13 Å tunnel, which is an average distance measured from residues at the pocket entrance (Tyr188, Pro213, and Tyr355). **(d)** EanB•hercynine binary complex (hercynine in cyan stick, shown in the omit map of hercynine contoured at 3.0 σ. In this complex structure, the distance between Cys412 side-chain sulfur atom and ε-carbon of hercynine is ~4.8 Å. **(e)** Alignment between the apo-EanB (orange) with EanB•hercynine binary complex (blue) shows high similarity between the two structures with r.m.s. derivate value of 0.14 Å. **(f)** The stereo view figure of EanB ɦercynine with Cys412 in persulfide form. The interaction network of hercynine and residues was shown in dash. **(g)** The different view of EanB ɦercynine with Cys412 in persulfide form. Key interactions are shown in dash line with distance labeled in (Å).

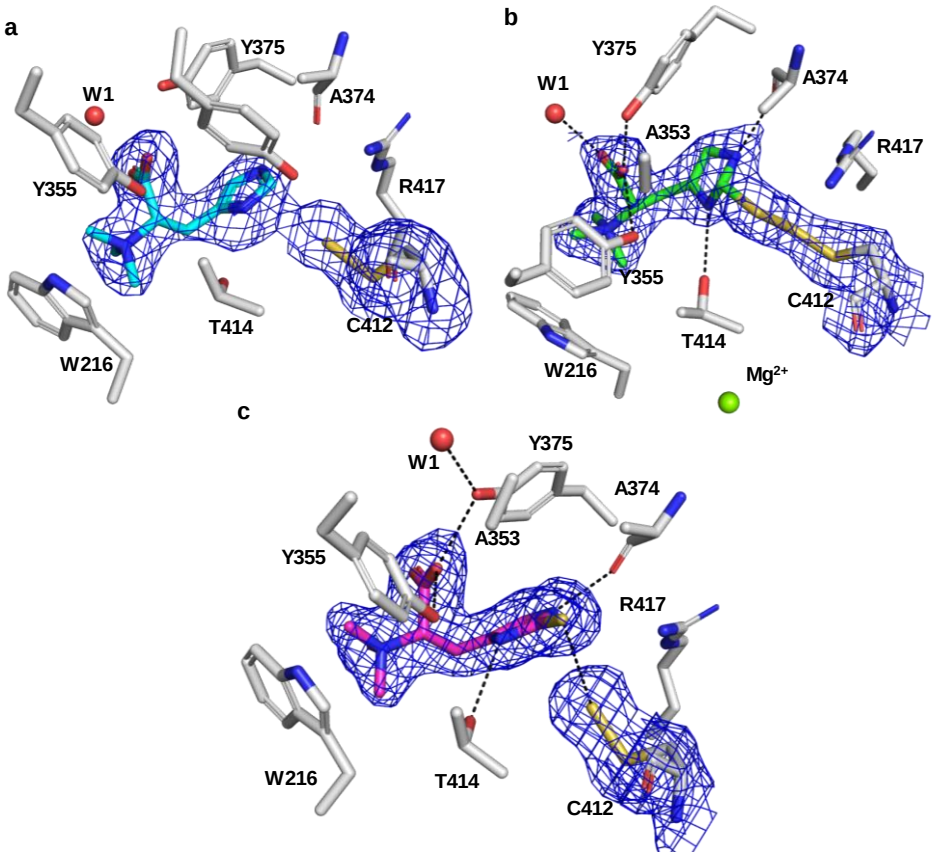

Figure S10 Electron density omit maps of crystal structures of under three stages in EanB catalysis shown in Figure 4. (a) EanB•hercynine binary complex with Cys412 persulfide intermediate. The electron density omit map is contoured at 3.0σ. The distance between terminal sulfur of Cys412 persulfide and ε-carbon of hercynine (cyan stick) is 3.2 Å. This structure is most likely the EanB•hercynine•persulfide intermediate immediately before the sulfur-transfer reaction. **(b)** The electron density omit map contoured at 3.0σ for the $EanB_{Y353A}$•hercynine•Cys412 trisulfide tetrahedral intermediate (green stick) showing the imidazole ring in non-planar geometry. **(c)** The electron density omit map contoured at 3.0σ for the $EanB_{Y353A}$•ergothioneine•Cys412 persulfide shows ergothioneine (magenta stick) has formed.

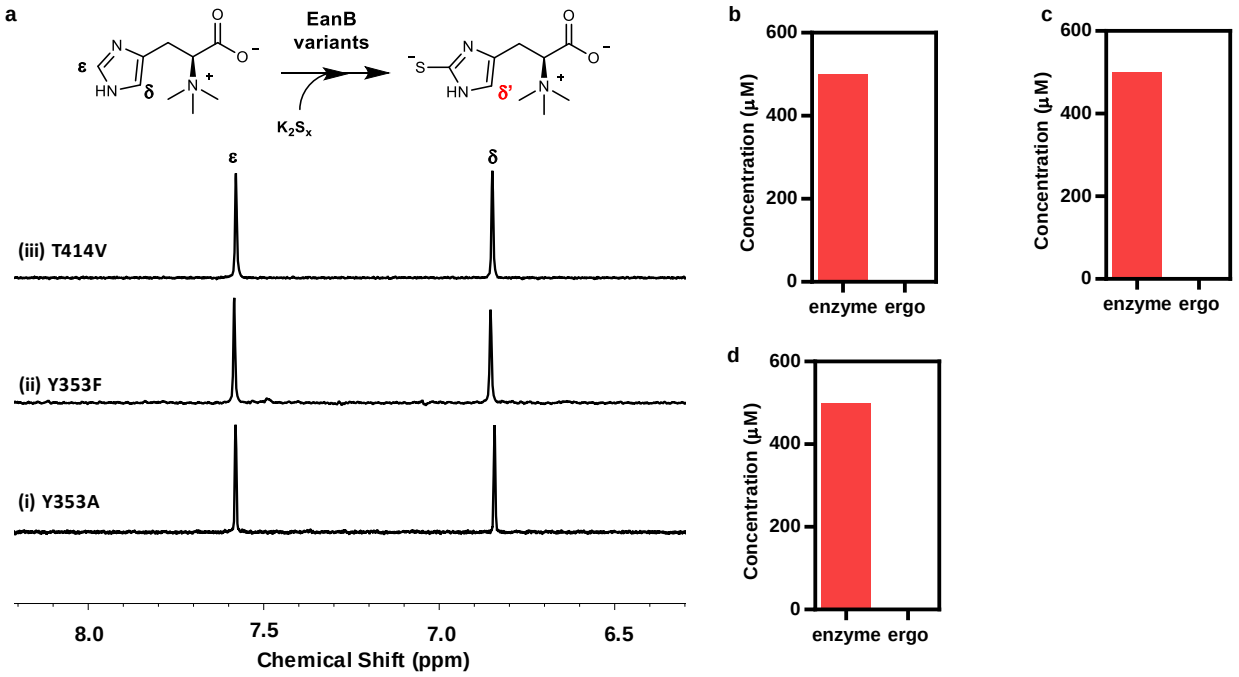

Figure S11 Characterization of EanB variants. (a) ^{1}H-NMR assay for $EanB_{Y353A}$, and $EanB_{Y353F}$, and $EanB_{T414V}$ variants' single-turnover reactions shows no detectable ergothioneine production **(b)-(d)** Quantitative mass spectrometry measurement of ergothioneine produced from these single-turnover reactions with K_2S_x as the sulfur source indicated that the amount of ergothioneine is less than 1% of the proteins of for $EanB_{Y353A}$, and $EanB_{Y353F}$, and $EanB_{T414V}$ variants used, respectively. **(b)** In $EanB_{Y353A}$ reaction, enzyme concentration was 500 μM and the amount of ergothioneine produced was 1.6 μM (~0.3% conversion. **(c)** In $EanB_{Y353F}$ reaction, enzyme concentration was 500 μM and the amount of ergothioneine produced was 0.02 μM (~ 0.004% conversion). **(d)** In $EanB_{T414V}$ reaction, enzyme concentration was 500 μM and the amount of ergothioneine produced was 0.53 μM (~ 0.1% conversion).

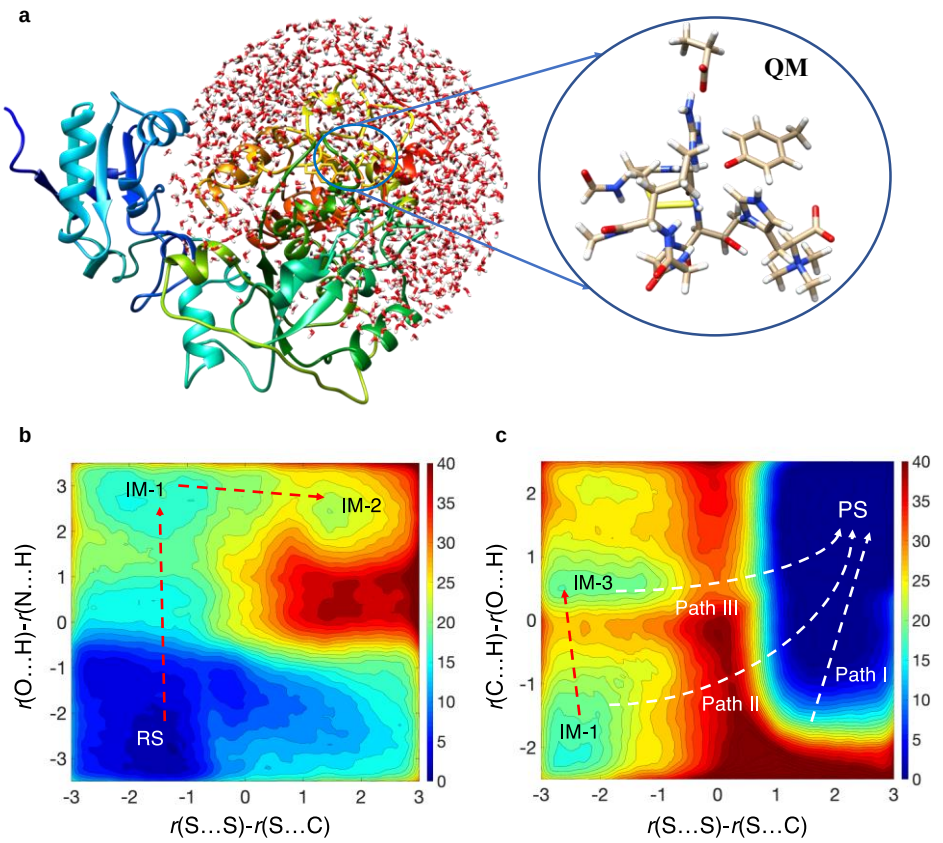

Figure S12 QM/MM study of the sulfur transfer process of in EanB-catalysis. (a) The EanB QM/MM enzyme system used in the simulation: there are 134 atoms in QM region described by the DFTB3/3OB-1 method. **(b-c)** 2D potential of mean force (PMF) obtained from QM/MM metadynamics simulation. In Path I, the protonation of hercynine by Tyr353 results in a metastable intermediate IM-1. The subsequent Cys412 persulfide nucleophilic attack and formation of C-S bond on the hercynine side-chain results in a tetrahedral intermediate (IM-2). In Path II, a concerted mechanism shows the formation of C-S bond together with the protonation of Tyr353 (TS). In Path III, the deprotonation of H imidazole by Tyr353 (IM-1) occurs prior to the C-S bond formation, which involves a carbene intermediate (IM-3). For the PMF shown in **(c)**, the C-H repulsive potential is re-parameterized based on proton affinity calculations (see **Table S2**). For additional discussions, see **Supporting Discussion.**

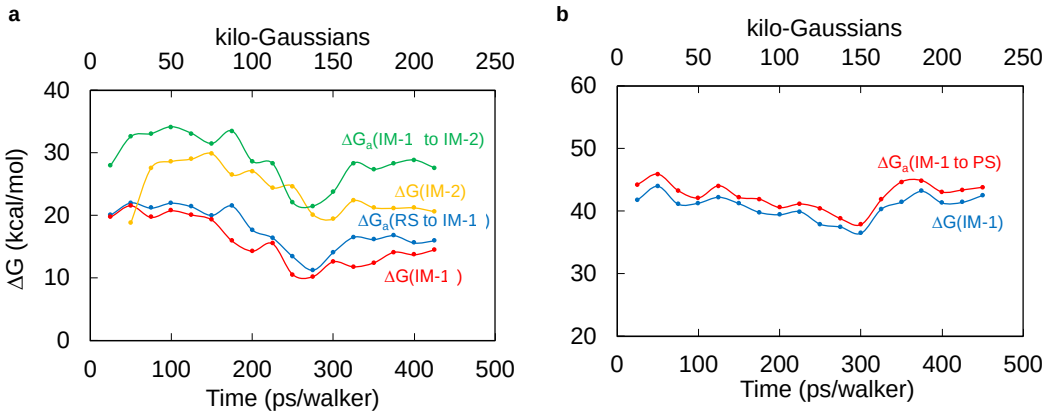

Figure S13 Convergence of QM/MM free energy simulations. (a-b) Convergence of relative free energies in metadynamics simulations. The simulations were performed for ~20 ns for each possible mechanism (about 400 ps or more for each walker). Convergence of relative free energies in metadynamics simulations. Each step used different number of walkers in the multi-walkermetadynamics, but each walker deposited Gaussians at the same rate. (a) deprotonation of Tyr353 and nucleophilic attack of persulfide to the ε-C atom of the substrate (free energy measured relative to the reactant state); (b) disulfide bond breakage and proton transfer back to the deprotonated Tyr353 (free energy measured relative to the product state).

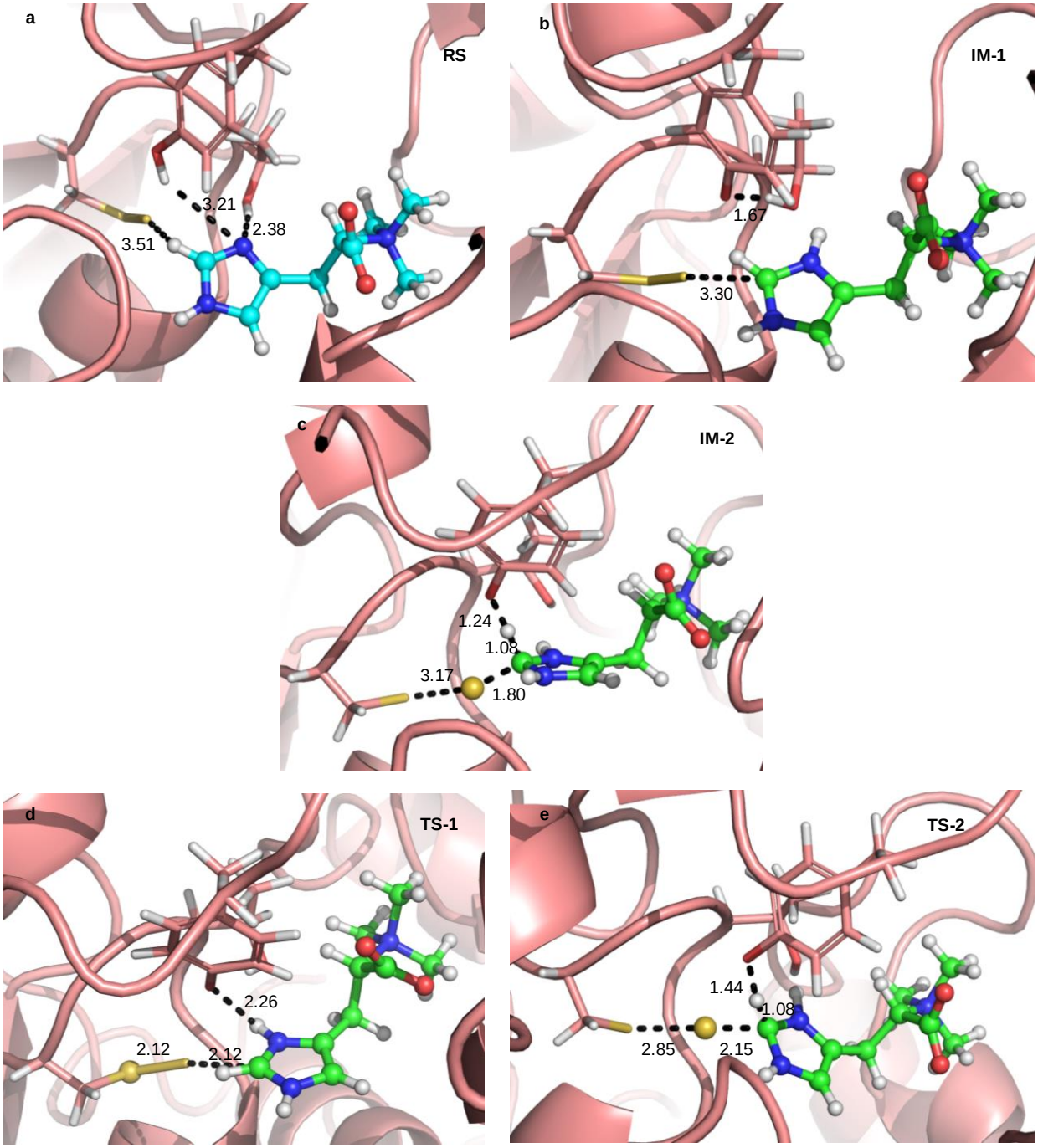

Figure S14 Representative snapshots for key species sampled during metadynamics simulations. These key species were sampled during metadynamics simulations for the free energy surface shown in Figure S12b: **(a)** the reactant state (RS); **(b)** the metastable intermediate IM-1 formed after the deprotonation of Tyr353; **(c)** the tetrahedral intermediate (IM-2); **(d)** the transition state (TS-1) for the formation of IM-1; **(e)** the transition state (TS-2) for the nucleophilic attack and formation of the tetrahedral intermediate (IM-2).

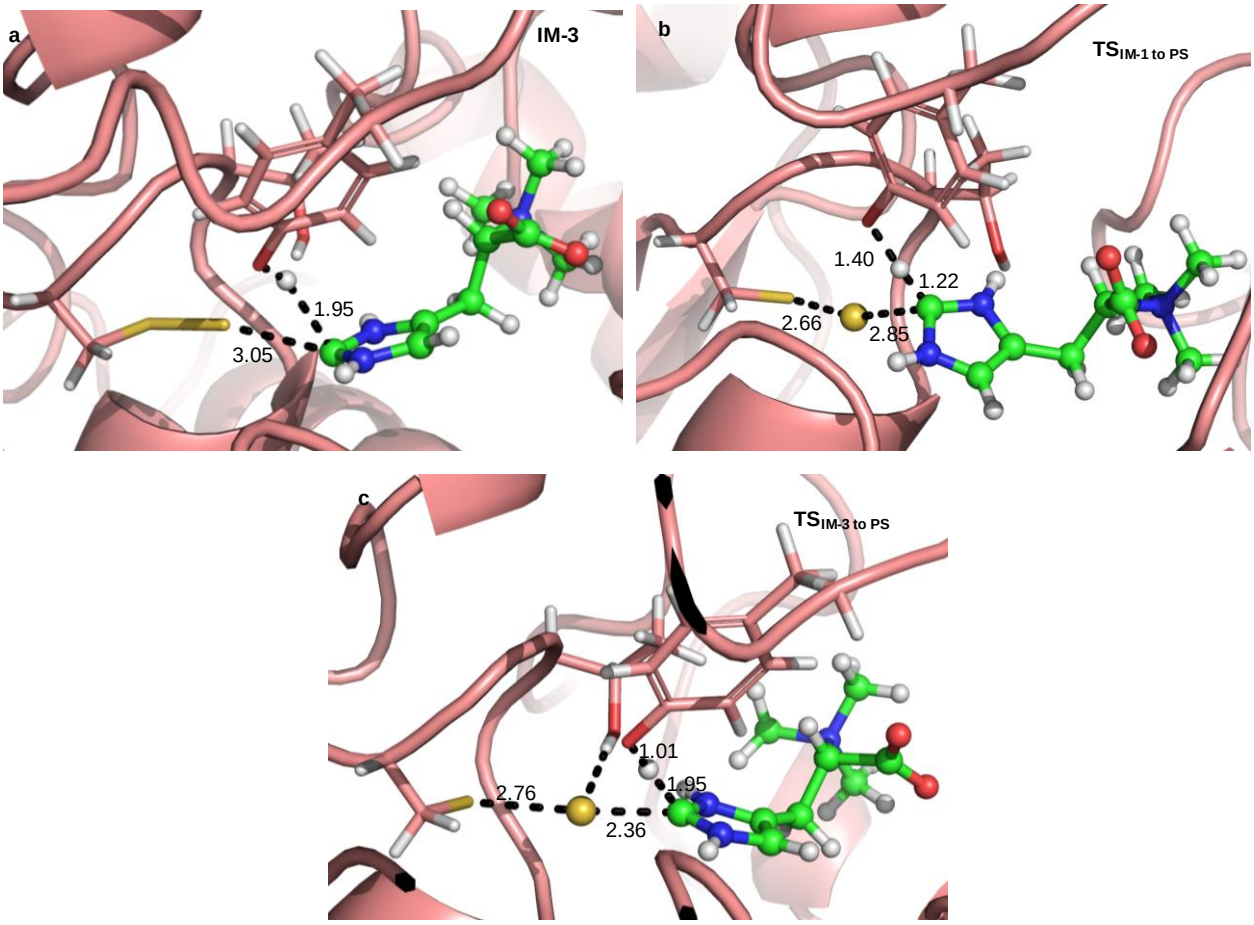

Figure S15 Representative snapshots for key species sampled during metadynamics simulations. These key species were sampled during metadynamics simulations for the free energy surface shown in Figure S12c: **(a)** the carbene intermediate formed in Path III (IM-3); **(b)** the transition state ($TS_{IM\text{-}1\ to\ PS}$) for the concerted pathway (Path II); **(c)** the transition state ($TS_{IM\text{-}3\ to\ PS}$) for the formation of product (PS) through Path III, which involves a carbene intermediate (IM-3).

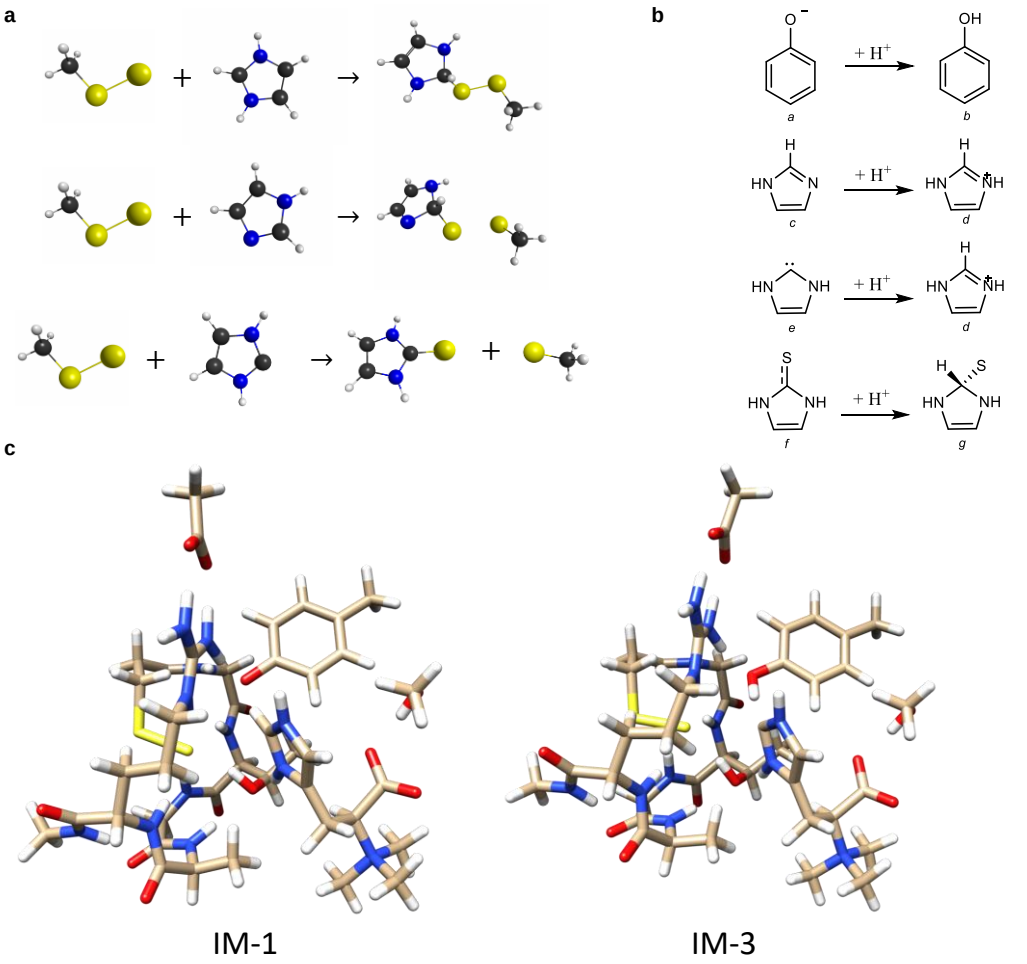

Figure S16 Model systems used to examine the reliability of DFTB3 for the reactions relevant to the EanB system considered. (a) Reaction between persulfide with an imidazole in different protonation states. **(b)** proton affinity of key species; **(c)** Optimized structures of possible intermediates during the nucleophilic attack reaction (IM-1 and IM-3, 136 atoms) at CPCM/B3LYP-D3/6-31G(d,p) level of theory.

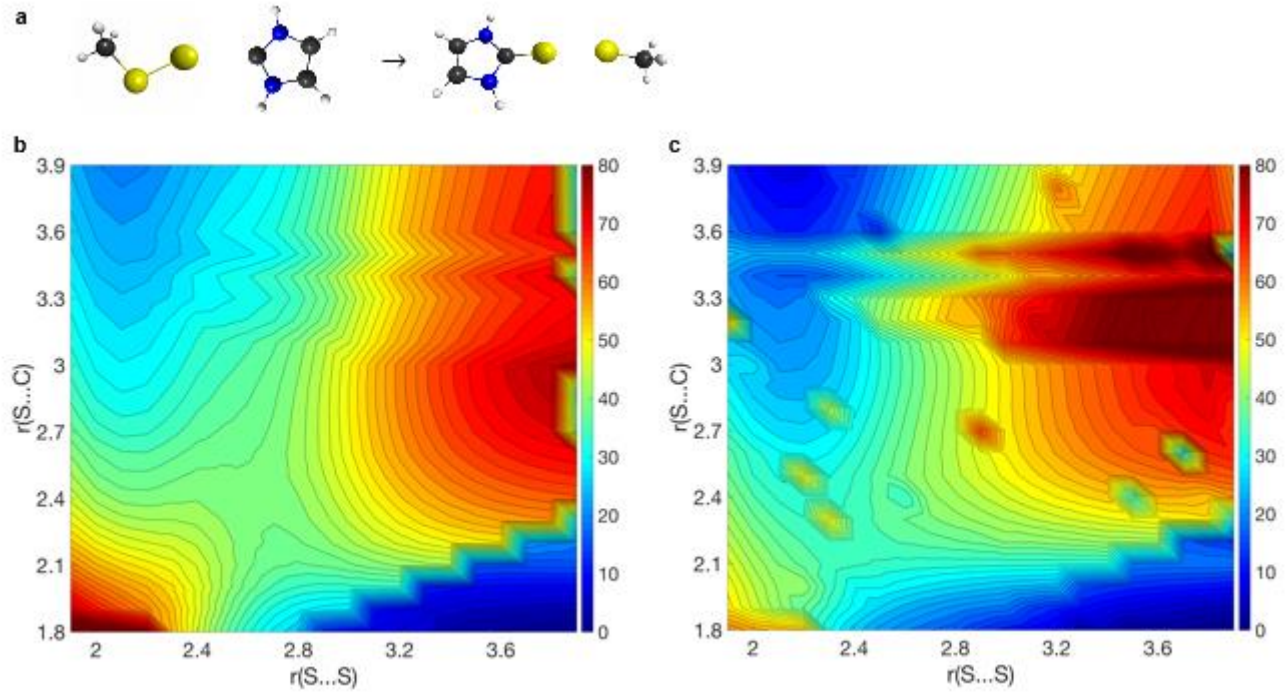

Figure S17 Adiabatic mapping by using DFTB3 and B3LYP-D3/6-311++G(d,p) methods. (a) Reaction between carbene and persulfide. **(b)** Potential energy surface at DFTB3 level of theory. **(c)** Potential energy surface at B3LYP-D3/6-311++G(d,p) level of theory with DFTB3 minimized structures.

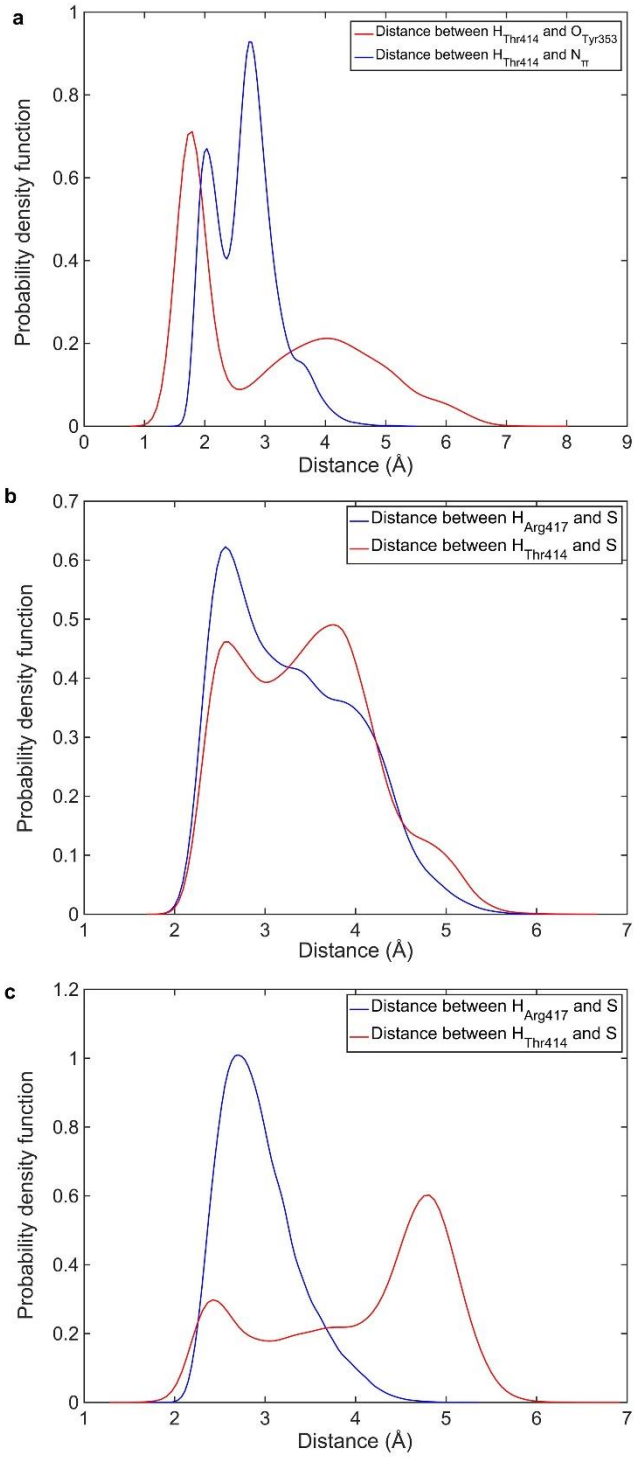

Figure S18 The probability density functions of key distances from metadynamics simulations: (a) for the distance between H_{Thr414} and O_{Tyr353} and the distance between H_{Thr414} and N_{π} atom of the substrate during the metadynamics simulation for the free energy surface shown in Figure S12b and S12c; **(b)-(c)** for the distance between H_{Thr414} and S_{Cys412} and the distance between H_{Arg417} and S_{Cys412} during different metadynamics simulations. **(b)** distances obtained from simulations for the free energy surface shown in Figure S12b; **(c)** distances obtained from simulations for the free energy surface shown in Figure S12c.

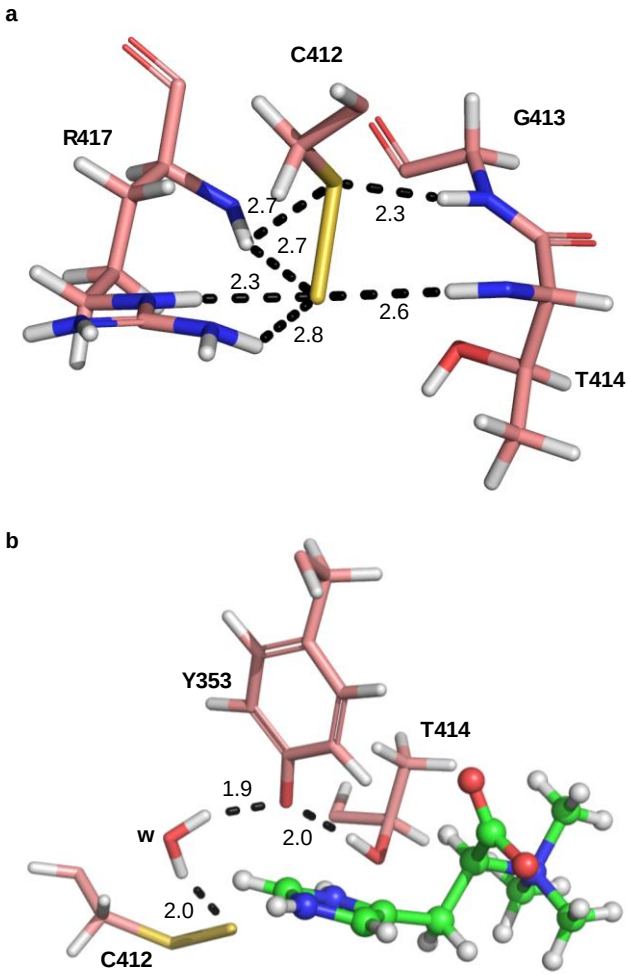

Figure S19 Sample snapshots from metadynamics simulations to illustrate: (a) Hydrogen bond network that stabilizes the persulfide species in the reactant state; **(b)** A water molecule migrates into the active site to stabilize the persulfide and the deprotonated Tyr353.

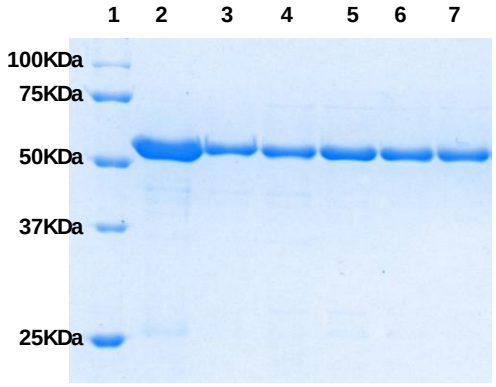

Figure S20 SDS-PAGE of anaerobic purified EanB and various mutant used in this work. The order of the samples was: (1) marker; (2) EanB wild type; (3) $EanB_{Y353A}$; (4) $EanB_{Y353F}$; (5) $EanB_{C412S}$; (6) $EanB_{T414V}$; and (7) $EanB_{C412\text{-only}}$.

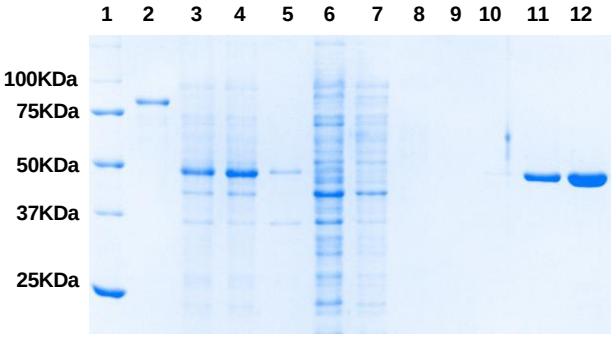

Figure S21 SDS-PAGE of purified ergothionase. The order of the samples was (1) marker; (2) in-house protein quantification standard; (3) cell lysate; (4) supernatant; (5) cell pallet resuspension; (6) flow through; (7) 1st resin volume of column wash fraction; (8) 4th resin volume of elution fraction (9) 7th resin volume of elution fraction (10) last resin volume of column wash fraction; (11) combined protein elution fraction (12) protein fraction after dialysis

Supporting Discussion

Additional discussion of free energy simulations

In the free energy simulations shown in **Figure S12b**, the hercynine ε-carbon C-H bond is constrained; otherwise three-dimensional free energy simulations will be computationally prohibitive even with the semi-empirical QM method employed here. In the additional free energy simulation shown in **Figure S12c**, hercynine ε-carbon C-H bond is no longer constrained, while the newly formed N_{π}-H bond in either IM-1 or IM-2 is constrained instead. The free energy surface for proton transfer from the substrate ε-carbon back to Tyr353 is largely downhill. Starting from IM-2, this proton transfer (Path I in the main text **Figure 4d**) is, in fact, barrierless. Then, from the metastable intermediate IM-1, two pathways are feasible. In the main text **Figure 4d** Path II, C-S bond forms in concert with proton transfer from hercynine ε-carbon back to the deprotonated Tyr353. In the main text **Figure 4d** Path III, a carbene intermediate may be involved (IM-3). The free energy surface indicates that the conversion from IM-1 to IM-3 involves a barrier comparable to the IM-1 to IM-2 conversion. The final product of ergothioneine is highly stable, more than 40 kcal•mol^{-1} below the reactant state. Carbene intermediates have been proposed in thiamine diphosphate dependent enzymes[5] and orotidine 5′-phosphate decarboxylase.[6]

The reliability of DFTB3 for the EanB system

To evaluate the reliability of the DFTB3 method for the EanB system, we have conducted several types of calculations using small molecule models (**Figure S16**).

First, we studied a reaction for the formation of a tetrahedral intermediate starting with a persulfide and an imidazole in different protonation states, as shown in **Figure S16a**. With a protonated imidazole, the reaction energy is -94.3 kcal•mol^{-1} at the DFTB3 level of theory. This compares favorably to the B3LYP-D3/6-31G(d,p) result of -97.0 kcal•mol^{-1} and the B3LYP-D3/6-311++G(d,p) result of -95.0 kcal/mol. With a neutral imidazole, the reaction energy is 27.3 kcal•mol^{-1} and 41.4 kcal•mol^{-1}, at the DFTB3 and B3LYP-D3/6-311++G(d,p) levels, respectively. These results suggest that the nucleophilic attack by the persulfide requires protonation of the imidazole ring, and that DFTB3 captures this effect adequately.

Second, we studied the proton affinity of key proton donor/acceptors involved in the elementary reaction steps (**Figure S16b**). The results in **Table S2** indicate that DFTB3 tends to overestimate the proton affinity by 4-9 kcal•mol^{-1} as compared to the G3B3 method; the major exception is the proton affinity of the ε-C in a doubly protonated imidazole, which is underestimated by DFTB3 as compared to both B3LYP and G3B3 calculations. Therefore, for the proton transfer between Tyr353 and the substrate, the relative proton affinities are adequately described by DFTB3, with the expected error in the range of 4-5 kcal/mol; this is the case for the first proton transfer from Tyr353 to the substrate N_{π} atom, and the proton transfer from the tetrahedral intermediate back to the deprotonated Tyr353. However, the error is likely significant for the proton transfer from ε-C in a doubly protonated imidazole back to Tyr353, since the errors in proton affinities are in the opposite direction and therefore add up (4+11=15 kcal•mol^{-1}!). As a result, we expect that the barriers associated with C-H bond breaking in IM-1 being substantially underestimated with the standard DFTB3/3OB level of theory. Thus, we used electronic energies obtained at the MP2/aug-cc-pVQZ level of theory to reparametrize the C-H repulsive potential in DFTB3/3OB. With this modification, the proton affinity of the ε-C in a doubly protonated imidazole at DFTB3 level of theory is comparable to both B3LYP and G3B3 calculations; the modified C-H repulsive potential model is used in PMF calculations

shown in **Figure S12c**.In addition , we note above that DFTB3 underestimates the difficulty for the sulfur transfer to a neutral imidazole (i.e., Path I), thus with all the errors in DFTB3 considered, Path II and III would remain at least competitive to pathway I , which is in accordance with the PMFs shown in **Figure S12**. Therefore, while more accurate QM/MM free energy simulations are required to draw firm conclusions regarding the relative importance of the three pathways, which will be presented elsewhere, the key values of the DFTB3/MM simulations are to highlight the importance of substrate protonation for the subsequent persulfide reaction and to propose plausible reaction mechanisms that are in semi-quantitative agreement with all experimental data in hand.

We note that Path III in **Figure S12** involves an unexpected intermediate, IM-3, which features a carbene-like electronic structure; it is formed after the substrate ε-C loses its proton to Tyr353 prior to the nucleophilic attack by the persulfide. To establish whether such an intermediate from DFTB3/MM simulations is also observed at a higher level of theory, we optimized the structures of IM-1 and IM-3 at the CPCM/B3LYP-D3/6-31G(d,p) level of theory. As shown in **Figure S16c** and **Table S3**, both species are indeed stable local minima on the DFT potential energy surface. In Path III, The energy barrier for the conversion of IM-1 to IM-3 is 14.8 kcal•mol^{-1} at the CPCM/B3LYP-D3/6-31G(d,p) level of theory, suggesting that the deprotonation of ε-C and re-protonation of Tyr353 is energetically feasible. In the subsequent step, i.e. the conversion of carbene intermediate (IM-3) to the product, the energy barrier is 22.1 kcal•mol^{-1} at the CPCM/B3LYP-D3/6-31G(d,p) level of theory. In Path II, the energy barrier for the conversion of IM-1 directly to PS is 26.5 kcal•mol^{-1} at the CPCM/B3LYP-D3/6-31G(d,p) level of theory, which is 4.4 kcal•mol^{-1} higher than that of Path III (with a carbene intermediate), suggesting that the Path II (as shown in **Figure S12)** may not be the favorable pathway. These data further support that a carbene intermediate may be involved in the catalytic reaction and the rate-limiting step can be the C-S bond formation starting from the carbene intermediate (IM-3) to the product.

As shown in **Table S3**, key geometrical parameters for all species obtained from DFTB3/MM metadynamics simulation are comparable to those optimized at the CPCM/B3LYP-D3/6-31G(d,p) level of theory. These results further support the use of DFTB3/MM for probing the reaction mechanism in the EanB system.

In addition, we studied the reaction for the formation of product with a persulfide and a carbene, as shown in **Figure S17a**. The reaction energy is -40.3 kcal•mol^{-1} at DFTB3 level of theory. This is close to that calculated at the B3LYP-D3/6-311++G(d,p) level of theory (-40.2 kcal•mol^{-1}). These results suggest that the reaction between carbene and persulfide is intrinsically favorable. To gain further understanding of the reaction process, two-dimensional potential energy surface was scanned at DFTB3 level of theory, as shown in **Figure S17b**. The potential energy surface features a well-defined saddle point that corresponds to an energy barrier of ~40.2 kcal•mol^{-1}. By using DFTB3 minimized structures, the potential energy surface (PES) was also computed at the B3LYP-D3/6-311++G(d,p) level of theory (**Figure S17c**), which shows an energy barrier of ~35.8 kcal•mol^{-1}. These results suggest that the formation of a carbene intermediate is plausible, and that DFTB3 is reliable for describing the reaction that involves this mechanism.

The role of Thr414

Experimental studies observed that mutation of Thr414 significantly reduces the enzymatic activity. This observation is consistent with findings from QM/MM simulations that Thr414 actively participates in the reaction. First, in the reactant state (RS, as shown in **Figure S14a**), Thr414 forms a hydrogen bond with the N_π

atom of the substrate, thus orienting the hercynine substrate for productive proton transfer with Tyr353. Second, once Tyr353 is deprotonated, Thr414 form a hydrogen bond with the deprotonated Tyr353, thus stabilizing the resulting intermediate (IM-1) as well as the transition state. These interactions are reflected by the probability density functions for the distance between H_{Thr414} and O_{Tyr353} and the distance between H_{Thr414} and N_{π} (**Figure S18a**), which indicate that during most of the simulation, H_{Thr414} features short hydrogen bond distances (1.5 Å to 2.1 Å) with either O_{Tyr353} or the N_{π} atom of the hercynine substrate.

In addition, compared to Tyr353, the alcohol group of Thr414 has a higher pKa and therefore is less favorable to donate the proton. We examined this possibility by using QM cluster models as discussed in the Computational Methods. Results show that the intermediate with a deprotonated Thr414 is not stable and readily falls back to the reactant state. Therefore, Thr414 is not a favorable proton donor in the reaction.

Moreover, during the persulfide nucleophilic attack, we observe that Thr414 forms a hydrogen bond with the Cys412 persulfide, suggesting that Thr414 also plays an important role in stabilizing the nucleophilic sulfur of the Cys412 persulfide (**Figure S18b** and **18c**). On the other hand, Thr414 is not the only key residue that stabilizes the sulfur atom. For example, Arg417 also plays an important role in this regard, as reflected by the distribution of corresponding hydrogen bonding distances (**Figure S18b** and **18c**). In addition, the backbone N-H of Gly413, Thr414 and Arg417 in α-helix 18 also interact with the persulfide, as shown in **Figure S19a**.

It is worth noting that a water molecule can migrate into the active site to replace the role of Arg417, mostly when Tyr353 is deprotonated (i.e. in the IM-1 state). This water molecule can form a hydrogen bond with either the persulfide ion or Tyr353. An example is shown in the snapshot in **Figure S19b**.

References

(1) Kamyshny, A.; Ekeltchik, I.; Gun, J.; Lev, O., Method for the Determination of Inorganic Polysulfide Distribution in Aquatic Systems. *Anal. Chem.* **2006**, *78*, 2631-2639.

(2) Kamyshny, A.; Goifman, A.; Gun, J.; Rizkov, D.; Lev, O., Equilibrium distribution of polysulfide ions in aqueous solutions at 25 ℃: a new approach for the study of polysulfides equilibria. *Environ. Sci. Technol.* **2004**, *38*, 6633-6644.

(3) Wood, J. L., Sulfane sulfur. *Methods Enzymol.* **1987**, *143*, 25-29.

(4) Leisinger, F.; Burn, R.; Meury, M.; Lukat, P.; Seebeck, F. P., Structural and mechanistic basis for anaerobic ergothioneine biosynthesis. *J. Am. Chem. Soc.* **2019**, *141*, 6906-6914.

(5) Meyer, D.; Neumann, P.; Ficner, R.; Tittmann, K., Observation of a stable carbene at the active site of a thiamin enzyme. *Nat. Chem. Biol.* **2013**, *9*, 488-490.

(6) Miller, B. G.; Wolfenden, R., Catalytic proficiency: the unusual case of OMP decarboxylase. *Annu. Rev. Biochem.* **2002**, *71*, 847-885.